Invited Paper

Development of an electrostatic levitator and containerless processing of metals, alloys, and semiconductors

Won-Kyu Rhim*
Jet Propulsion Laboratory, California Institute of Technology, M/S 183-401
4800 Oak Grove Drive, Pasadena, CA 91109

ABSTRACT

Present capability of the High Temperature Electrostatic Levitator (HTESL) at JPL for the containerless materials processing is described. The capability includes the measurements of various thermophysical properties and the studies of undercooling and nucleation phenomena. The thermophyscial properties that can be measured include the density, the volume expansion, the ratio between the specific heat capacity and the hemispherical total emissivity, the surface tension, the viscosity, the spectral emissivity, and the electrical resistivity. For liquids where the Wiedemann-Franz-Lorenz law applies, their thermal conductivities can be determined indirectly from the electrical resistivities. The capability of determining the statistical nature of nucleation and the Temperature-Time-Transformation (T-T-T) curves has also been demontrated. Experimental results on pure metals, alloys, and semiconductors were use to support the argument.

Keywords: Electrostatic levitator, thermophysical properties, undercooling and solidification, molten metals and semiconductors, density, specific heat, surface tension, viscosity, electrical resistivity, hemispherical total emissivity

1. INTRODUCTION

Suspending a small (micron size) charged particle by the electrostatic forces has a long history. Since the celebrated oil drop experiment of R. A. Millikan in 1909, there has been a number of papers published on the subject of charged particle suspension [1-5]. However, none of these works have addressed the problems of levitating large objects for the purpose of studying drop dynamics or measuring thermophysical properties at high temperatures.

The development of the high temperature electrostatic levitator (HTESL) described in this paper was initiated at JPL in 1989, and the feasibility was demonstrated in 1992 [6]. Since then, non-contact diagnostic techniques have been developed for the measurements of various thermophysical properties. At the present time, thermophysical properties that can be measured by the HTESL at JPL include the density, the volume expansion, the ratio between the specific heat capacity and the hemispherical total emissivity, the surface tension, the viscosity, the electrical resistivity, and the spectral emissivity.

This paper begins with a brief description of electromagnetic levitator (EML), the conventional high temperature levitator which in many ways has the similar characteristics to the HTESL. Then the principle of operation of the HTESL at JPL will be briefly described. The following sections are devoted to the application of the HTESL for various thermophysical property measurements, and for the studies of the undercooling/nucleation and the kinetic properties of undercooled liquids. Description of each capability was supported by the actual experimental data that have been obtained using the JPL-HTESL. Emphasis were laid on the escription of the basic principles while the details of the measurement processes were referred to the earlier publications.

2. ELECTROMAGNETIC LEVITATION

In an electromagnetic levitator, a conductor sample is placed in a suitably designed coil which is energized by the radio frequency (RF) power. The applied RF field interacts with the induced currents in the sample to produce forces which keep the sample in the middle of the coil. In this process, the induced currents heat the sample, and this heating mechanism is commonly used to raise the sample temperature.

The advantages of electromagnetic levitators are that they can levitate conducting materials either in a vacuum or in a controlled gas environment. Electromagnetic levitators have been extensively used to study solidification phenomena from undercooled liquids. The capability of inducing crystalline nucleation at a predetermined undercooled state makes it possible to measure the solidification velocity and to study the formation of metastable crystalline phases.

* Correspondence: E-mail: won-kyu.rhim@jpl.nasa.gov; Tel: 818-354-2925; FAX: 818-393-5039

However, electromagnetic levitators have limitations for the measurements of thermophysical properties. One of the main limitations is in its inability to separate the levitation forces from the heating of the sample. The electromagnetic levitation force is proportional to the gradient of the applied magnetic field, i.e. grad·B. while the sample heating is proportional to the square of the same magnetic field, B^2. Such a heating poses the lower limit in the sample temperature. Inert gas streams are often used to overcome the limit, taking risks of contaminating the sample. Under such a circumstance, the energy balance equation is given by

$$mc_p \frac{dT}{dt} = -\varepsilon_T \sigma A(T^4 - T_S^4) - hA(T - T_S) + Q_{rf}, \quad (1)$$

where m is the sample mass, T is the sample temperature, T_s is the temperature of surroundings, ε_T is the hemispherical total emissivity, σ_{SB} is the Stefan-Boltzmann constant, A is the surface area of the sample, and c_p is the specific heat capacity. h is the heat transfer coefficient which accounts for the conductive and the convective cooling in the gas stream, and Q_{rf} is the RF power absorbed by the sample. In contrast, the levitation forces in an electrostatic levitator do not affect the sample temperature. It operates in a high vacuum, thus making the heat transfer equation very simple eliminating the last two terms in Eq. (1). HTESL heats the sample using a radiant heat source. When the heating beam is blocked, the entire cooling curve can be expressed by the radiative heat transfer equation:

$$mc_p \frac{dT}{dt} = -\varepsilon_T \sigma A(T^4 - T_S^4), \quad (2)$$

providing the basis for the accurate measurement of ε_T/c_p since the all other parameters in the equation are either already known or accurately measurable.

Another characteristic of the electromagnetic levitation operating on the ground is its vigorous stirring of the sample melt caused by the induced currents. Sometimes such a stirring may be beneficial to homogenize the melts. However, it may also cause instabilities in sample shape and induce various sample motions which will make it difficult to accurately measure the thermophysical properties such as the mass density, the surface tension, or the viscosity.

3. HIGH TEMPERATURE ELECTROSTATIC LEVITATOR [6]

In an electrostatic levitator, a charged sample is positioned at a preset point by applying appropriate electrostatic fields to the sample. Since electrostatic field cannot have a three-dimensional potential minimum according to the Earnshaw's theorem[7], sample positioning is only possible by actively controlling the applied electric fields at least in one direction. In our system this is accomplished by adopting a feedback-control, whereby any deviation of sample position from a preset position is automatically corrected. The basic principle of electrostatic levitation is illustrated in Fig. 1. A charged sample is positioned between a pair of circular disk electrodes, while the sample position is monitored by a position sensor, and the position information is fed to a micro-computer which generates an appropriate control signal.

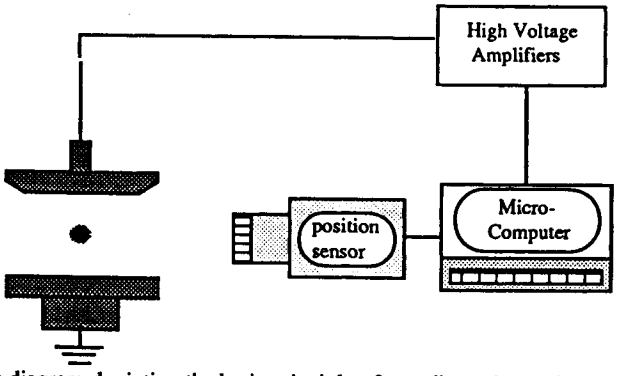

Fig. 1. Schematic diagram depicting the basic principle of one dimensional electrostatic levitation.

This signal is amplified and supplied to the top electrode in order to generate the electric field that is required to keep the sample position maintained at a desired position. A sample that is levitated in the middle of the electrodes in the 1-g environment should satisfy the force-balance equation given by

$$mg = \frac{Q_s V}{L}, \tag{3}$$

where m is the mass of the sample which carries surface charge Q_S, and V is the voltage difference between the disk electrodes which are separated by a distance L. For example, if $Q_S = 0.69 \times 10^{-9}$ Coulomb, m = 140 mg, and L = 10 mm, the required potential difference between the two electrodes is approximately 10 kilo-volts. The sample charge is inversely proportional to the levitation voltage which can be measured by a voltmeter. Importance of sample charge in conjunction with determination of correct surface tension will be explained later.

The levitator shown in Fig. 1 controls the sample position along the vertical direction while it relies on a two dimensional potential well in the lateral directions. Therefore, the sample may be oscillating in the lateral potential well unless feedback controls are also implemented in these directions. A schematic diagram of an electrode assembly which was designed for the three dimensional position controls is shown in Fig. 2. In addition to a pair of parallel circular disk electrodes, two pairs of small side electrodes surround the bottom disk electrode. Two separate position control signals are applied to these electrodes in order to damp the oscillatory motions in lateral directions. As before, the top electrode is connected to a high voltage amplifier which supplies the vertical levitation field, and the bottom electrode is electrically grounded through an AC amplifier. When it is needed, the AC amplifier generates oscillating electric fields across the disk electrodes and induce resonant oscillations on a levitated drop [8]. The four coils positioned on the top electrode, when they are energized, produce a rotating horizontal magnetic field which can induce sample rotation around the vertical axis [9]. The electrode assembly is housed by a stainless steel chamber that is typically evacuated to a $\sim 10^{-8}$ Torr.

A schematic diagram of the levitation chamber is shown in Fig. 3. The chamber is surrounded by various equipment which support the sample levitation, sample heating, and various diagnostics for thermophysical properties measurements. Two mutually orthogonal position detectors detect the sample images to produce three-dimensional position information. This position information is processed by a micro-computer, and the three output signals, after amplification, are distributed to appropriate electrodes for sample position control. Keeping the sample very stable throughout an experiment is extremely important for sample heating as well as directing diagnostic instruments.

A 1-kilowatt UV-rich high-pressure xenon arc-lamp is used for the initial sample heating. A fused quartz lens is used to focus the beam onto the sample, and a spherical mirror that is placed at the opposite side of the lens in order to collect the light beam that misses the sample. This lamp can be used to raise the sample temperature to a final sample temperature, or it can be switched by a 100 Watt YAG laser when the sample reaches the thermionic temperature [10]. With the YAG laser, temperatures in excess of 2500 K can be reached.

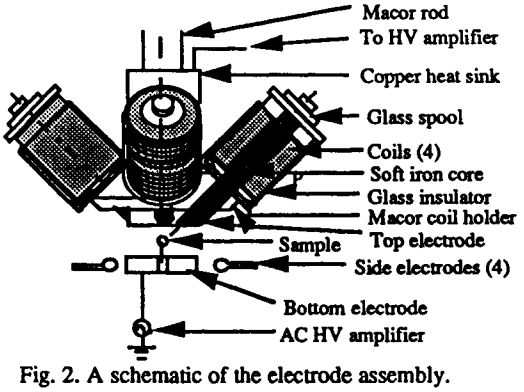

Fig. 2. A schematic of the electrode assembly.

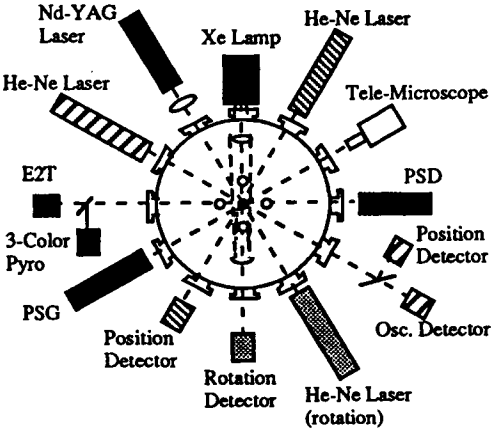

Fig. 3. Schematic diagram of the HTESL at JPL.

In the HTESL, the positive sample charge is maintained utilizing the photoelectron and/or the thermionic electron emission. These charging mechanisms ensure enough sample charges for the levitation in the presence of neutralizing space charges. Below the thermionic temperature (~1200°C), the photoelectric emission ensures the sample charge, while the thermionic charging kicks in when the sample temperature exceeds the thermionic temperature.

4. MEASUREMENTS OF MASS DENSITY AND THERMAL EXPANSION [11, 12]

Mass density is one of the fundamental parameters which affects other thermodynamic quantities. HTESL has suitable characteristics for the density measurements: (i) First of all, quiescent sample levitation helps taking crisp sample images. (ii) Molten samples levitated by HTESL show slightly prolate spherical shapes which are axi-symmetric around the vertical direction. Therefore, full information about the drop volume can be obtained from a single side image of the drop. The underlying definitions for the density ρ and the thermal expansion coefficient β are given by

$$\rho = m/V,$$

$$\beta = \frac{1}{V}\frac{\partial V}{\partial T},$$

where m is the sample mass, V is the sample volume, and T is the sample temperature.

The basic process of density measurement consists of (i) digitization of recorded video images, (ii) edge detection from the digitized image, (iii) calculation of the area (or the sample volume), and (iv) calibration of the data with respect to a reference sphere for absolute sample volume. A detailed description of the density measurement method can be found in the earlier publications [11, 12].

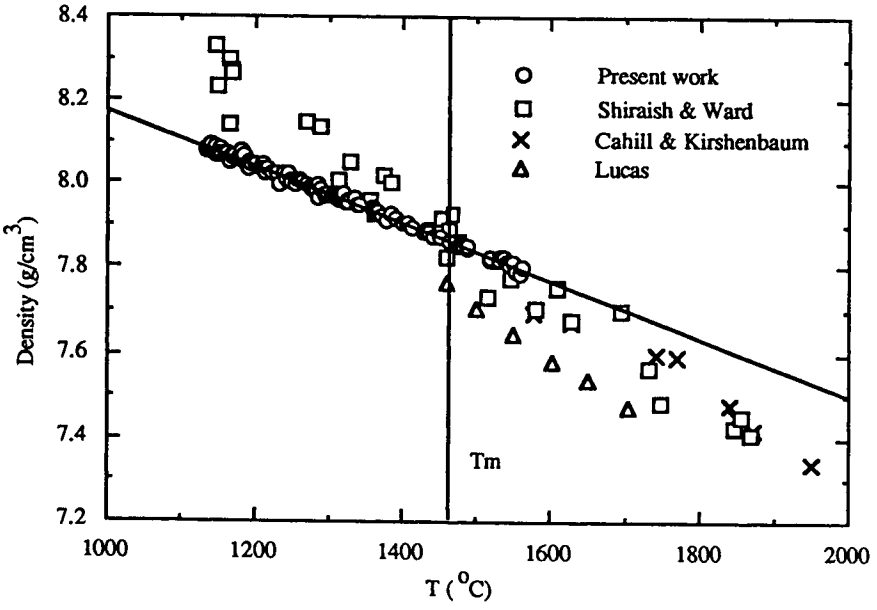

Fig. 4. Density of molten nickel obtained by the HTESL [11, 12]. It was compared with earlier studies that used EML (Shiraishi), maximum bubble pressure (Lucas), and Archimedian (Cahill and Kirshenbaum) methods.

The density measurement system consists of a high quality tele-microscope, a CCD video camera attached to the tele-microscope, a video recording system, and a mini-computer for image digitization and analysis. Image analysis software was developed to extract the image area accurately. As an example, Fig. 4 shows the density of pure nickel which was obtained using the HTESL at JPL, and was compared with results from the literature [13-15]. To obtain these results, the nickel sample was heated to ~100K above its melting point. Then the melt was allowed to cool with the heating beam was suddenly

blocked. During the cooling process both the sample temperature and the video images were recorded simultaneously. The melt undercooled more than 300K before it recalesced.

Fig. 5 shows the density of molten silicon. Over the temperature range 1350 K < T < 1850 K, the data show a quadratic nature. Such quadratic behavior of liquid silicon density was observed for the first time in our measurements [16, 17]. Also shown in Fig. 5 is the volume expansion that was derived from the density data. Finally, Fig. 6 shows the specific volumes of four Ni-Zr alloys[18]. The melting point of each alloy is indicated by the arrow. Specific volumes of $Ni_{24}Zr_{76}$ alloy are very close to but slightly smaller than those of $Ni_{36}Zr_{64}$ alloy. It is interesting to note that the specific volume of $NiZr_2$ is significantly smaller than those of the other alloys. This density measurement technique was also applied to a bulk glass-forming alloy $Zr_{41.2}Ti_{13.8}Cu_{12.5}Ni_{10.0}Be_{22.5}$ [19] and to a pure zirconium[10].

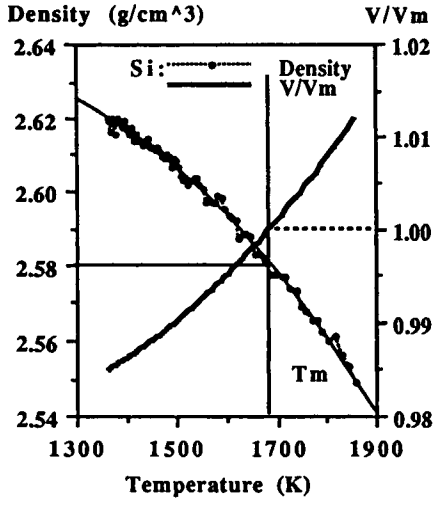

Fig. 5. Density and volume expansion of molten Si.

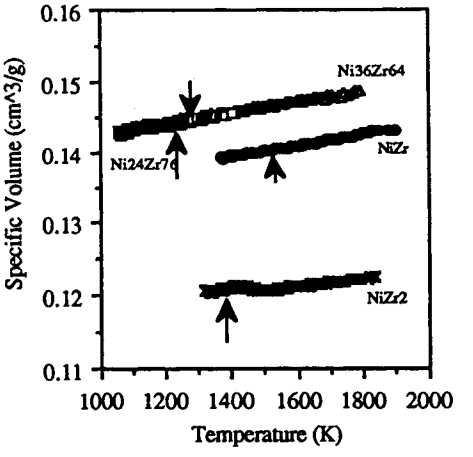

Fig. 6. Specific volumes of four Ni-Zr alloys

5. HEAT CAPACITY AND HEMISPHERICAL TOTAL EMISSIVITY [20, 21]

Specific heat capacity is an important thermodynamic quantity from which other thermodynamic parameters can be derived. However, the heat capacity data of high temperature liquids are either lacking or inaccurate even if they exist in the literature. Data is particularly scarce for undercooled liquids since they immediately solidify when placed in contact with crucibles.

Knowledge on hemispherical total emissivity ε_T is important when one has to calculate the radiant heat flux. For instance, ε_T determines the thermal environment during crystal growth in the floating zone growth system, and also in determining the cooling rate of atomized droplets in rapid solidification process. The hemispherical total emissivity of a sample is defined by the ratio between the hemispherical total emissive power H to that of a black body, i.e.

$$\varepsilon_T = \frac{H}{\sigma_{SB} T^4}. \tag{4}$$

In HTESL, the ratio between the specific heat capacity and the hemispherical total emissivity c_p/ε_T can be obtained from the heat transfer equation that describes the radiative cooling in absence of heat inputs. From Eq. (2), c_p/ε_T can be expressed by

$$\frac{c_p}{\varepsilon_T} = -\frac{6\sigma_{SB}(T^4 - T_R^4)}{\rho d \frac{dT}{dt}}. \tag{5}$$

Since both T and dT/dt can be obtained from a cooling curve, c_p/ε_T can be readily obtained from this equation. For example, Fig. 6 shows a cooling curve of a molten silicon. From the liquid portion of the curve, both T and dT/dt were extracted to determine c_{pl}/ε_T from Eq. (5). The results are shown in Fig. 7 [16]. Note that unlike pure metals such as nickel and zirconium[10, 20, 21], the molten silicon shows nonlinear temperature dependence. Such temperature dependence is probably related to changes in short-range atomic order in the undercooled melts.

From the $c_p(T)/\varepsilon_T(T)$ data, $c_p(T)$ can be determined if $\varepsilon_T(T)$ is known. Likewise, $\varepsilon_T(T)$ can be determined if $c_p(T)$ is known. Strictly speaking $\varepsilon_T(T)$ has to be measured independently if it is to be used to determine $c_p(T)$. However, in an environment where $\varepsilon_T(T)$ is not available, $c_p(T_m)$ at the melting temperature can be used to determine $\varepsilon_T(T_m)$. In a special circumstance where the assumption $\varepsilon_T(T) \equiv \varepsilon_T(T_m)$ can be made over a temperature interval, $c_p(T)$ can be determined from the $c_p(T)/\varepsilon_T(T)$ over that interval.

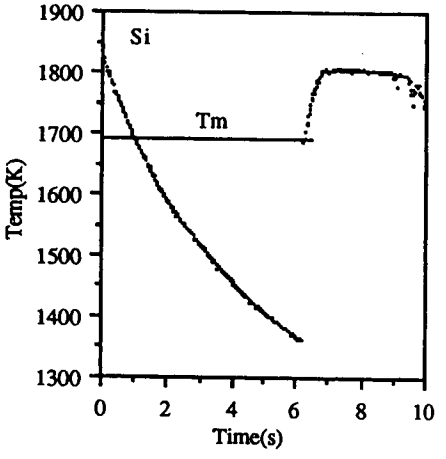

Fig. 7. A cooling curve of a molten silicon [16].

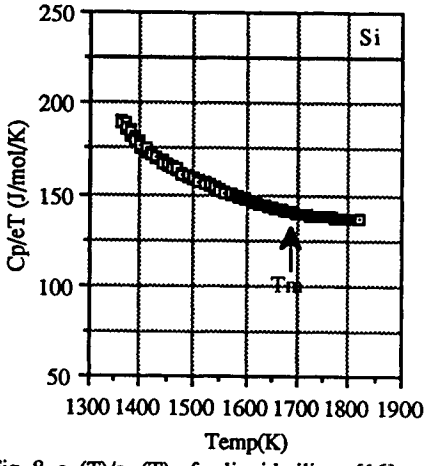

Fig. 8. $c_p(T)/\varepsilon_T(T)$ of a liquid silicon [16].

6. MEASUREMENTS OF SURFACE TENSION AND VISCOSITY [8, 22-24]

The spherical shape of the molten samples levitated by the HTESL greatly simplify the surface tension measurements with high accuracy. Since the HTESL operates in a high vacuum environment, it helps to maintain a clean sample surface condition. This is important due to the fact that surface tension is particularly sensitive to even a minute surface contamination. If a liquid drop has a low viscosity, in the small amplitude limit, a free oscillation motion can be expressed by

$$r(t) = r_o + \sum_{2}^{\infty} r_n \cos(\omega_n t) P_n(\cos\theta) \exp(\frac{-t}{\tau_n}), \tag{6}$$

where r_0 is the radius of the drop when it assumes spherical shape, P_n (cos θ) is the Legendre polynomial of order n, θ is the angle measured between z axis and the radial direction, r_n is the oscillation amplitude of n-th mode. The characteristic oscillation frequency corresponding to the n-th mode is given by [25]

$$\omega_n = n(n-1)(n+2)\frac{\sigma}{\rho r_o^3}(1 - \frac{Q_e^2}{64\pi^2 r_o^3 \sigma \varepsilon_o}), \tag{7}$$

where n = 2, 3, 4, ..., σ is the surface tension, ρ is the density of the drop, Q_S is the surface charges, and ε_0 is the permittivity of vacuum. Thus, from the characteristic oscillation frequency for the n=2 mode, the surface tension can be determined by

$$\sigma = \frac{r_*^3 \rho}{8}(\omega_2^2 + \frac{Q_S^2}{8\pi^2 r_*^6 \rho \varepsilon_*}). \tag{8}$$

The shape of a drop that is levitated by an electrostatic force against the gravity deviates in various degrees from a perfect sphere depending upon the size and the amount of charge on the drop. Equilibrium shapes and stability of a charged conducting drop levitated by a uniform electric field was analyzed by Adornato and Brown [26] whose asymptotic analysis for the equilibrium drop shape in small electric fields showed the appearance of the second and third Legendre functions. The correction term which accounts for such imperfections was calculated by Feng and Beard [27] using an analytic multiple parameter perturbation method.

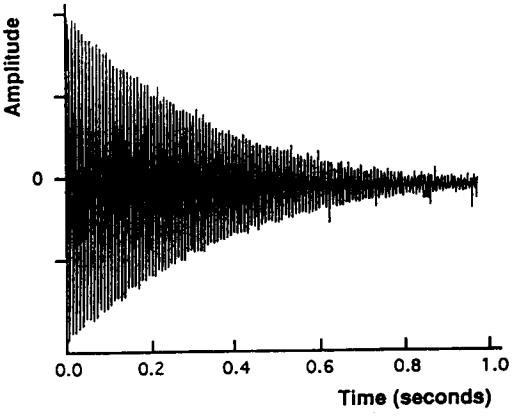

Fig. 9 A transient oscillation signal of a nickel-zirconium alloy [8].

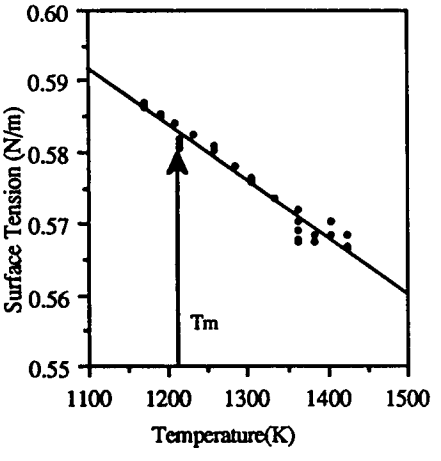

Fig. 10. Surface tension of molten germanium[29].

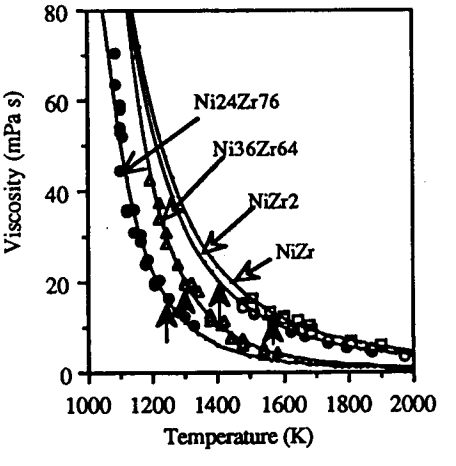

Fig. 11. Viscosities of four Ni-Zr alloys [18].

According to Lamb, the damping time constants shown in Eq. (4) are given by [28]

$$\frac{1}{\tau_n} = (n-1)(2n+1)\frac{\eta}{\rho r_*^2}, \tag{9}$$

where η is the viscosity of the sample liquid. For n=2 mode, the viscosity is given by

$$\eta = \frac{\rho r_e^2}{5\tau_2}. \tag{10}$$

The drop oscillation was induced by applying a low level AC voltage to the bottom electrode. When the frequency matches the resonance frequency of the drop, the drop starts to oscillate. When the excitation field is suddenly truncated, the drop oscillation freely decays. Fig. 9 shows a typical transient oscillation at n = 2 mode obtained from a molten Ni-Zr drop. Such signals are detected and analyzed for the frequency and the decay time constant. The oscillation frequency is related to the surface tension through Eq. (8) while the damping time constant is related the viscosity through Eq. (10). Fig. 10 shows the surface tension of molten germanium [29] so obtained, and Fig. 11 shows the viscosities of nickel-zirconium alloys of four different compositions [18]. Both the surface tension and the viscosity of molten zirconium have also been successfully measured down to the deeply undercooled state [10, 30].

The surface tension measurement technique described in this section can be applied to liquids which have relatively lower viscosity. When the liquid viscosity exceeds a certain critical value, the damping constant become so short that the oscillation frequency cannot be determined with meaningful accuracy. When this situation happens, a new technique for the surface tension measurement becomes necessary.

7. MEASUREMENT OF ELECTRICAL RESISTIVITY[9]

The basic principle of asynchronous induction motor was used to measure the relative changes of electrical resistivity of levitated samples. The four-coil assembly shown in Fig. 1 works as a stator while the levitated sample serves as a rotor. According to the principle of the induction motor [31, 32], if an AC voltage E_1 at frequency ω_s is applied to a stator (having a resistance R_1 and an inductance L_1), the torque τ experienced by the rotor (having its own resistance R_2 and inductance L_2) that is rotating at an instantaneous rotation frequency ω is given by

$$\tau = \frac{\omega_s E_1^2}{R_1^2 + \omega_s^2 L_1^2}\left(\frac{sR_2}{R_2^2 + s^2 L_2^2}\right), \tag{11}$$

where

$$s \equiv \frac{\omega_s - \omega}{\omega_s}. \tag{12}$$

Since the condition $R_2^2 >> s^2L^2$ is satisfied in our experiment, Eq. (11) assumes a simpler form:

$$\tau = \left(\frac{\omega_s E_1^2}{R_1^2 + \omega_s^2 L_1^2}\right)\frac{1}{R_2}\left(1 - \frac{\omega}{\omega_s}\right). \tag{13}$$

This equation shows that, when the left parenthesis (the stator term) is kept constant, the measured torque decreases linearly as a function of the rotor frequency, and its gradient is inversely proportional to the resistance of the rotor.

Validity of this technique was demonstrated using an aluminum sample around its melting temperature [9]. To measure the resistivity, the torque was measured as a function of temperature, inverted them, and calibrated them with respect to a reference point (24.185 $\mu\Omega$·cm) given in the literature [33]. Fig. 12 shows the resistivity of aluminum obtained around the melting temperature.

Since both the solid and molten aluminum are conductors where free electrons are responsible for the electrical and thermal conductivities, one can use the Wiedemann-Franz-Lorenz Law to convert the electrical resistivity to thermal conductivity:

$$\frac{\kappa_{liq} r_{liq}}{T} = \frac{\pi^2 k^2}{3e^2} \equiv L_o = 2.45 \times 10^{-8} \quad \text{W}\Omega\text{K}^{-2}, \tag{14}$$

where k is the Boltzmann constant and e is the electron charge. The constant $L_0 = \pi^2 k^2 / 3e^2$ is the Lorenz number whose validity was experimentally confirmed with high accuracy by Busch et al.[34]. When this law was applied to the resistivity data of Fig. 12, the corresponding thermal conductivities are as shown in Fig. 13. These results agree quite well with the literature values. This method was also successfully applied to a molten germanium [29].

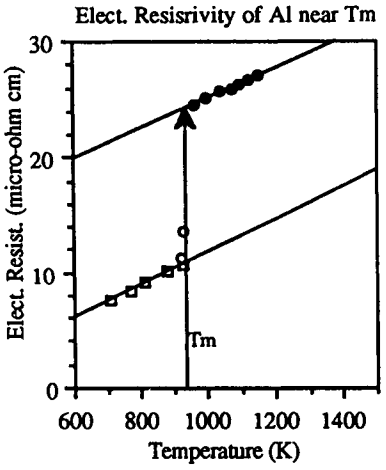

Fig. 12. Electrical resistivity of aluminum around the T_m.

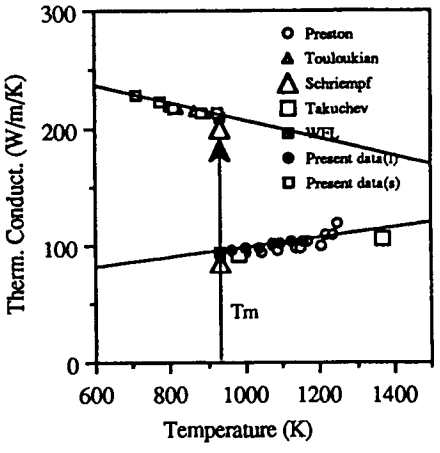

Fig. 13. Thermal conductivity of aluminum determined from Fig. 12 using the W-F-L law.

8. STUDIES OF UNDERCOOLING AND NUCLEATION [35, 36]

Statistical phenomena of nucleation in undercooled liquids can be studied using the HTESL. In transient undercooling experiments, a molten sample at a preset temperature is radiatively cooled by suddenly blocking the heating source, and statistical distribution of undercooling temperature is recorded and analyzed. For a given sample, the fastest cooling rate can be attained when the heating beam is blocked. If it is needed, cooling rate can be further increased by reducing sample size since the cooling rate is inversely proportional to the sample radius. The HTESL at JPL was used for the first time to investigate the statistics of nucleation using molten zirconium drops of two different purities, and the results were analized using the classical nucleation theory [35]. The HTESL also allows to study the nucleation phenomena in steady-state undercooled liquids, and to determine the Time-Temperature-Transformation curves. Such experiment was successfully carried out using a glassforming alloy ($Zr_{41.2}Ti_{13.8}Cu_{12.5}Ni_{10.0}Be_{22.5}$) [36]. The capabilities of measuring nucleation statistics as well as the required thermophysical properties [37, 38] makes the HTESL a powerful tool for the investigation of the entire nucleation phenomena.

9. DROP ROTATION AND A NEW METHOD FOR SURFACE TENSION MEASUREMENT [39]

For low viscosity liquids, the drop oscillation method is an adequate non-contact surface tension measurement method [8]. However, if the viscosity of a liquid exceeds a certain critical value, the drop oscillation method cannot be used, and development of a new non-contact technique is required. Based on the shape deformation of rotating drops, a new technique for the surface tension measurement was developed at JPL [39]. For a drop that is undergoing steady state rotation, the degree of deformation at a given rotation frequency depends on the surface tension of the liquid.

Brown and Scriven predicted that the shape of a drop undergoing solid-body rotation should initially follow an axisymmetric branch until it reaches the bifurcation point, at which the drop shape transforms from an axisymmetric to a triaxial ellipsoidal shape[40]. Fig. 14 shows both the theoretical curve and the experimental data which were obtained using a molten aluminum drop that was levitated by the HTESL. From this figure, if the shape parameter R_{max}/R_0 and the rotation frequency ω_{rot} are known, one can determine the effective oscillation frequency, ω_{osc}, at any point in the axisymmetric branch. Once the effective frequencies ω_{osc} are determined, the surface tension can be calculated following the same recipe given in the

previous section (Section 6). Since $\omega_{rot}/\omega_{osc}$= 0.559 at the bifurcation point, ω_{osc} can determined if ω_{rot} is measured at the bifurcation point. This approach for the surface tension measurement should be applicable to liquids regardless of their viscosities as long as the solid-body rotation condition is observed.

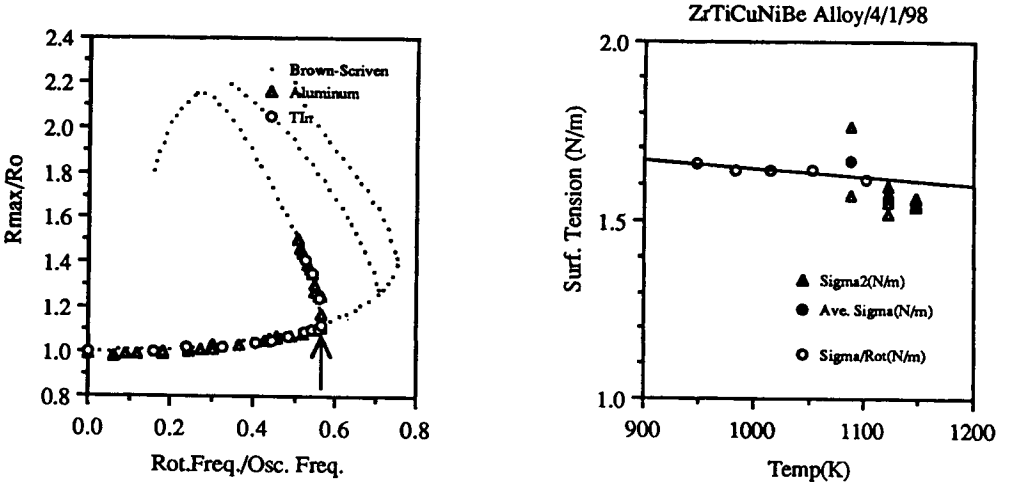

Fig. 14. Normalized maximum dimension of a rotating drop as a function of rotation frquency normalized with respect to the oscillation frequency of the drop in non rotating state.

Fig. 15. Surface tension of a glass forming alloy ($Zr_{41.2}Ti_{13.8}Cu_{12.5}Ni_{10.0}Be_{22.5}$). The open circles are the surface tensions measured using the drop rotation technique, while the triangles are the data taken by the oscillation method. The solid circles are the averages of the drop oscillation data.

This new technique was applied to a bulk glass-forming alloy ($Zr_{41.2}Ti_{13.8}Cu_{12.5}Ni_{10.0}Be_{22.5}$). This alloy had such a high viscosity that the drop oscillations could not be induced below 1080K (T_m=993K). Fig. 15 shows the surface tension of the alloy that was measured using the new technique along the surface tension data which were obtained using the drop oscillation technique. The open circles were obtained using the drop rotation method while the triangles were from the drop oscillation method. One can observe in this figure that accuracy of the drop oscillation method when the temperature was lowered, and then it reached a critical temperature below which drop oscillation could not be induced any longer. Detailed description of this technique is described in the reference [39].

6. SUMMARY AND DISCUSSION

The present capabilities of the HTESL at JPL were outlined. The description of its capability was supported by the actual experimental data that have been obtained using the JPL levitator, while the details were referred to earlier publications. Capabilities of the HTESL can be summarized in the following way:

(i) The HTESL can process a broad range of materials, including metals, semiconductors and some insulators. Maintaining sufficient charges on the sample surface is the only requirement to generate the levitation forces. In contrast, the EML is limited to relatively good electrical conductors.

(ii) In the HTESL, the sample heating and the levitation do not interfere with each other so that the sample temperature can be varied over a wide temperature range, whereas the electromagnetic field in the EML is intrinsically coupled to the sample heating, thus, limiting the lowest temperature that can be attained for a given sample.

(iii) The processing environment being a high vacuum, the sample cooling in the absence of the heating can be rigorously described by the radiative heat transfer equation, allowing the accurate measurements of C_p/ε_T. In contrast, the EML uses an AC calorimetry to measure the same property.

(iv) The HTESL, through the employment of feedback control, provides a quiescent positioning during the sample processing, allowing the accurate measurements of thermophysical properties. Whereas, a molten sample levitated by an EML is subjected to a strong internal flow which may cause the shape distortion and instabilities, making it difficult to accurately measure the sample volume (or the density), the surface tension, and the viscosity.

(v) The HTESL provides a widely open view of levitated sample so that it can be viewed by various non-contact diagnostic instruments, whereas the levitation and heating coils in an EML are closely wound around the levitated sample, restricting access to the diagnostic instruments.
(vi) HTESL is already equipped with drop excitation techniques which can induce sample oscillations and rotations. These capabilities are needed for the studies of the drop dynamic, and the measurements of surface tension, viscosity, and electrical resistivity.
(vii) Drops levitated in the HTESL show slight asphericity, however, they are axisymmetric around the vertical direction. This allows accurate determination of the drop volumes (therefore liquid densities and thermal expansion coefficients if measured as a function of temperature) from a single side image of the drop.

ACKNOWLEDGMENTS

The authors would like to thank D. Elleman, M. Saffren, M. Collander, M Hyson, S. Chung, R. E. Spjut, D. Barber, K.-F. Man, A. Rulison, T. Ishikawa, and P.-F. Paradis who contributed in various degrees during the development and construction of the HTESL at JPL. The author would like express his special thanks to Dr. Paul-François Paradis for his critical reading of this manuscript. This work was carried out at the Jet Propulsion Laboratory, California Institute of Technology, under a contract with the National Aeronautics and Space Administration.

REFERENCES

1. P. J. Wyatt, and D. T. Phillips, J. Colloidal Interface Sci. 39, 125, 1972
2. S. Arnold, J. Aerosol Sci. 10, 49, 1979
3. L. Altwegg, M. Pope, S. Arnold, W. Y. Fowlkes, and M. A. El Hamamsy, Rev. Sci. Instru. 53, 332, 1982
4. M. R. Libera, P. P. Bolsaitis, R. E. Spjut, and J. B. Van der Sande: "Liquid supercooling and droplet cooling rates of remelted argon-atomized Fe-30Ni Powder Particles," J. Mater. Res. 3, 441, 1988
5. E. Bar-Ziv, D. B. Jones, R. E. Spjut, D. R. Dudek, A. F. Sarofim, and J. P. Longwell: "Measurement of combustion kinetics of a single char particle in an electrodynamic thermogravimetric analyzer" Combust. Flame 75, 81, 1989
6. W. K. Rhim, S. K. Chung, D. Barber, K. F. Man, Gary Gutt, A. Rulison, and R. E. Spjut. "An Electrostatic Levitator for High Temperature Containerless Materials Processing in 1-g," Rev. Sci. Instrum. 64, 2961-2970, 1993.
7. For Earnshaw's theorem, see, for example, S. A. Straton: *Electromagnetic Theory* (McGraw Hill, New York, 1941) p. 116
8. W. K. Rhim, K. Ohsaka, P.-F. Paradis, and R. E. Spjut, "A Non-Contact Technique of Measuring Surface Tension and Viscosity of Molten Materials using Electrostatic Levitation", Rev. Sci. Instrum. June 1999 (in press)
9. W. K. Rhim, and T. Ishikawa, "Noncontact Measurement of Resistivity of Molten Material", Rev. Sci. Instrum. 69, 3628-3633, 1998.
10. P.-F. Paradis, and W. K. Rhim, "Thermophysical Properties of Zirconium using Electrostatic Levitation", Proc. 1999 SPIE Conf. Denver, Colorado
11. S. K. Chung, D. Thiessen, and W. K. Rhim, "A Non-Contact Measurement Technique for the Density and Thermal Expansion of Molten Materials," Rev. Sci. Instrum. 67 (9) 3175-3181, 1996.
12. S. K. Chung, D. Thiessen, and W. K. Rhim, Erratum on "A Non-Contact Measurement Technique for the Density and Thermal Expansion of Molten Materials," Rev. of Sci. Instrum., 68, 1, 1997
13. S. Y. Shiraishi, and R. G. Ward, Can. Metall. Q. 3, 117, 1964.
14. A. D. Kirchenbaum, and J. A. Cahill, Trans. ASM 56,1963,281.
15. L.D. Lucas, Doctoral thesis, Univ. Paris, 1962.
16. W. K. Rhim, S. K. Chung, A. J. Rulison, and R. E. Spjut, "Measurements of Thermophysical Properties of Molten Silicon by a High Temperature Electrostatic Levitator", Int. J. Thermophysics 18 (2) 459-469, 1997
17. K. Ohsaka, S. K. Chung, W. K. Rhim, and J. C. Holzer "Densities of Si determined by an image digitizing technique in combination with an electrostatic levitator", Appl. Phys. Lett. 70,423-425, 1997
18. K. Ohsaka, S. K. Chung, and W. K. Rhim, "Specific volume and viscosity of the Ni-Zr alloys and their influence on the undercooling and glass forming capability of the alloys", Acta Materialia 46, 4535-4542, 1998
19. K. Ohsaka, S. K. Chung, and W. K. Rhim, A. Peker, D. Scruggs, and W. L. Johnson, "Specific volumes of the $Zr_{41.2}Ti_{13.8}Cu_{12.5}Ni_{10.0}Be_{22.5}$ alloy in the liquid, glass, and crystalline phases", Appl. Phys. Lett. 70 (6), 726-728, 1997.
20. A. Rulison, and W. K. Rhim, "Containerless Measurements of Specific Heat and Hemispherical Total Emissivity of Refractory Materials" Rev. Sci. Instrum. 65, 695-700, 1994
21. A. Rulison, and W. K. Rhim, "Constant Pressure Specific Heat to Hemispherical Total Emissivity Ratio for Undercooled Liquid Nickel, Zirconium and Silicon" Metall. & Mat. Trans. 26B: 503-508, 1995

22. W. K. Rhim, and A. J. Rulison, "Surface Tension and Viscosity Measurements by High Temperature Electrostatic Levitator", NASA Tech Brief, 64-65, July 1996
23. R. E. Spjut, and W. K. Rhim, "Software for Exciting Vibrations of Levitated Liquid Drops", NASA Tech Brief, 61, April 1997
24. R. E. Spjut, and W. K. Rhim, "Software for Analyzing Vibrations of Levitated Liquid Drops", NASA Tech Brief, 60, April 1997.
25. Lord Rayleigh, Phil. Mag. 14, 184, 1882.
26. P. M. Adornado, and R. A. Brown, Proc. R. Soc. London, A 389, 101, 1983.
27. J.Q. Feng, and K.V. Beard, "Small-amplitude of electrostatically levitated drops," Proc. Roy. Soc. (London), A, 430, pp. 133-150, 1990.
28. H. Lamb, *Hydrodynamics*, 6th ed., Cambridge University Press, 473-639, 1932.
29. W. K. Rhim, and T. Ishikawa, "Thermophysical Properties of Molten Germanium Measured by a High Temperature Electrostatic Levitator", The 5th Asian Thermophysical Properties Conference, August 30 - Sept. 2, 1998, Seoul, Korea, pp 611-616. Also submitted to Int. J. Thermophysics.
30. P-F. Paradis and W. K. Rhim, "Thermophysical Properties of Zirconium at High Temperatures", J. Mat. Research (submitted)
31. S. A. Nasar, and I. Boldea, *Electric Machines (Steady State Operation)*, Hemisphere Publishing Corporation, 1990.
32. P. L. Alger, *Nature of Induction Machine*, Gordon and Breach Science Publishers, 1965.
33. T. Iida and R. I. L. Guthrie, *The Physical Properties of Liquid Metals* (Clarendon press, Oxford), p. 228, 1988.
34. G. Busch, H. -J. Guntherodt, W. Haller, and P. Wyssmann, Phys. Lett. 43A, 225, 1973.
35. A. J. Rulison, W. K. Rhim, R. Bayuzick, W. Hofmeister, and C. Morton, "Containerless liquid to solid nucleation pathway in two representative grades of commercially available zirconium", Acta Materialia 45(3): 1237-1245, 1997.
36. Y. J. Kim, R. Busch, W. L. Johnson, A. J. Rulison, and W. K. Rhim, "Experimental determination of a time-temperature-transformation diagram of the undercooled $Zr_{41.2}Ti_{13.8}Cu_{12.5}Ni_{10.0}Be_{22.5}$ alloy using the containerless electrostatic processing technique" Appl. Phys. Lett. 68, 1057-1059, 1996
37. R. Busch, Y. J. Kim, W. L. Johnson, A. J. Rulison, W. K. Rhim, and D. Isheim, "Hemispherical total emissivity and specific heat capacity of deeply undercooled $Zr_{41.2}Ti_{13.8}Cu_{12.5}Ni_{10.0}Be_{22.5}$ melts", Appl. Phys. Letts. 66: 3111-3113, 1995
38. K. Ohsaka, S. K. Chung, and W. K. Rhim, A. Peker, D. Scruggs, and W. L. Johnson, "Specific volumes of the $Zr_{41.2}Ti_{13.8}Cu_{12.5}Ni_{10.0}Be_{22.5}$ alloy in the liquid, glass, and crystalline phases", Appl. Phys. Lett. 70 (6), 726-728, 1997.
39 W.K. Rhim and T. Ishikawa, "Rotating Molten Metallic Drops and Related Phenomena: a New Method for Measuring Surface Tension", Proc. 1999 TMS, Feb. 28- March 4, San Diego, CA.
40. R. A. Brown and L. E. Scriven, "The Shape and Stability of Rotating Liquid Drops", Proc. R. Soc. Lond. A 371, 331, 1980